

Artificial intelligence for context-aware visual change detection in software test automation

Milad Moradi*

AI Research, Tricentis, Vienna, Austria

m.moradi-vastegani@tricentis.com

ORCID: [0000-0002-9724-0339](https://orcid.org/0000-0002-9724-0339)

Ke Yan

AI Research, Tricentis, Sydney, Australia

k.yan@tricentis.com

David Colwell

AI Research, Tricentis, Sydney, Australia

d.colwell@tricentis.com

Rhona Asgari

AI Research, Tricentis, Vienna, Austria

r.asgari@tricentis.com

* Corresponding author. **Postal address:** Tricentis GmbH, Leonard-Bernstein-Straße 10, 1220 Vienna, Austria.

Abstract

Automated software testing is integral to the software development process, streamlining workflows and ensuring product reliability. Visual testing within this context, especially concerning user interface (UI) and user experience (UX) validation, stands as one of crucial determinants of overall software quality. Nevertheless, conventional methods like pixel-wise comparison and region-based visual change detection fall short in capturing contextual similarities, nuanced alterations, and understanding the spatial relationships between UI elements. In this paper, we introduce a novel graph-based method for visual change detection in software test automation. Leveraging a machine learning model, our method accurately identifies UI controls from software screenshots and constructs a graph representing contextual and spatial relationships between the controls. This information is then used to find correspondence between UI controls within screenshots of different versions of a software. The resulting graph encapsulates the intricate layout of the UI and underlying contextual relations, providing a holistic and context-aware model. This model is finally used to detect and highlight visual regressions in the UI. Comprehensive experiments on different datasets showed that our change detector can accurately detect visual software changes in various simple and complex test scenarios. Moreover, it outperformed pixel-wise comparison and region-based baselines by a large margin in more complex testing scenarios. This work not only contributes to the advancement of visual change detection but also holds practical implications, offering a robust solution for real-world software test automation challenges, enhancing reliability, and ensuring the seamless evolution of software interfaces.

Keywords: Software test automation, Artificial intelligence, Machine learning, Computer vision, Graph-based visual change detection

1. Introduction

Quality assurance in software development plays a pivotal role in ensuring the reliability, functionality, and overall excellence of software products [1, 2]. As the complexity of software systems continues to escalate, the significance of robust quality assurance practices becomes increasingly important. Quality assurance is a comprehensive process that spans the entire software development life cycle, from initial design and coding to testing and deployment. It involves systematic and meticulous testing, verification, and validation processes aimed at identifying and rectifying defects, bugs, and potential issues before a software product reaches end-users [3-5].

Software test automation holds immense importance in the realm of software development due to its capacity to enhance efficiency, reliability, and overall quality [6]. In the dynamic landscape of software development, ensuring the reliability and stability of applications through effective test automation methodologies is of paramount importance [7]. Visual change detection, a critical aspect of software testing, plays a key role in identifying alterations to the user interface, thereby facilitating the maintenance of software integrity. Visual testing can allow software developers and testers to find and fix visual regressions before they are released to end-user. Traditional methods often fall short in capturing nuanced interface changes, necessitating innovative approaches that can adapt to the evolving complexity of modern software systems.

In this paper, we introduce a novel method for visual change detection in software test automation, harnessing the power of Artificial Intelligence (AI), Machine Learning (ML), and graph-based analysis. Our approach addresses the challenges posed by intricate user interface structures by employing a ML model, i.e. You Only Look Once (YOLO) [8], to detect and accurately label User Interface (UI) controls within software screenshots. The detected controls serve as the building blocks for constructing a graph that encapsulates the spatial relationships between them, offering a holistic representation of the interface layout. Visual and textual information within detected controls are also utilized to have a context-aware representation of UI layout. In addition to the graph-based modelling of UI layout, we employ a novel similarity estimation algorithm to find corresponding nodes between graphs. This algorithm uses the similarity of neighbours within graphs to estimate how similar two given nodes are. Corresponding nodes between graphs represent the correspondence between UI controls in two software screenshots. This information about corresponding controls is eventually used to find changes in the UI.

We conducted extensive experiments to evaluate the performance of our change detector in various visual change detection scenarios. We created three datasets that simulate different situations of visual testing on web applications in two modalities (or platforms), i.e. desktop and mobile. We also implemented two baseline methods, i.e. pixel-wise comparison and region-based change detection, to compare their performance against our change detector. The experimental results showed that the pixel-wise comparison can only perform better than the other methods in very simple scenarios where the target and changed images come from the same modality and there is no resizing, cutting, and shifting in the images. However, our change detector is able to achieve high levels of precision and recall; it even outperformed the baselines in more complex visual testing scenarios. These results suggest that our change detection method can be efficiently and reliably used in a wide range of simple to complex visual testing use cases. This enables rapid detection of visual regressions, assessing contextual differences between various UI layouts of an application across different platforms, and enhancing the robustness of automated testing procedures.

The rest of this paper is organized as follows. In Section 2, we give an overview of related work in software test automation and AI-driven change detection in images. A detailed description of our graph-based visual change detection method is given in Section 3. We then present and discuss the experimental results in Section 4. Finally, concluding remarks are discussed and future lines of work are drawn in Section 5.

2. Related work

Software testing is a critical and integral component of the software development life cycle, playing an essential role in ensuring the quality, reliability, and functionality of software products [9]. Its importance lies in the systematic and thorough examination of software applications to identify defects, errors, or inconsistencies that may compromise performance or user experience. Effective testing not only validates that the software meets specified requirements but also helps detect and rectify issues early in the development process, preventing costly post-deployment problems. Moreover, software testing enhances user confidence by delivering products that are robust, secure, and free from critical bugs [10, 11]. In a rapidly evolving technological landscape, where software is a crucial part of every business and organization, the role of comprehensive testing is indispensable to deliver high-quality, dependable software solutions that meet the ever-growing expectations of users and stakeholders.

Automated software testing is a crucial facet of modern software development, offering efficiency, repeatability, and enhanced test coverage. Its importance lies in accelerating the testing process, reducing human errors, and enabling quick feedback loops during the development life cycle [12, 13]. Automated software testing is regarded as a solution to reduce testing costs and decrease cycle time in software development [14]. Furthermore, it can effectively discover vulnerabilities and failure points of software systems that may be accidentally or deliberately neglected by engineers or testers. Various techniques are employed in automated software testing, including unit testing, where individual components are tested in isolation; integration testing, ensuring the seamless collaboration of integrated components; and end-to-end testing, validating the entire software system's functionality. Additionally, regression testing helps maintain software integrity by swiftly detecting unintended side effects of code changes [15]. Continuous Integration (CI) and Continuous Deployment (CD) practices further leverage automated testing to ensure that software updates are thoroughly tested and seamlessly integrated into the development pipeline [16]. By combining these techniques, automated software testing contributes significantly to the delivery of high-quality software products, meeting the demands of today's fast-paced and dynamic development environments [15, 17].

AI and ML methods have various applications in different stages of software development lifecycle, for accelerating software requirements analysis, architecture design, implementation, testing, and maintenance [18]. Previously, AI has been utilized for automated software testing tasks such as discovering the behaviour of application under test, mapping application behaviour to test cases, error monitoring, self-healing, test case generation, test case prioritization, and other related tasks [19-22]. The application of AI in software test automation can revolutionize testing processes by enhancing efficiency and adaptability. AI-driven tools can autonomously generate test cases, analyse complex system interactions, and intelligently adapt test scenarios to evolving software architectures, significantly accelerating testing cycles and improving the overall quality of software products. In this paper, we also adopt an AI-driven approach towards software test automation, more specifically the task of visual testing.

Visual testing is a crucial aspect of software testing, particularly in the realm of UI and user experience (UX) validation. It focuses on assessing the visual aspects of a software application to ensure that it meets design specifications and remains aesthetically consistent across different environments and configurations [23]. In software testing and test automation, visual testing is indispensable for identifying graphical anomalies, layout issues, and unexpected changes in the user interface [24]. As applications become more visually intricate, the importance of visual testing intensifies, as it helps detect issues that traditional automated testing methods may

overlook. Visual testing is particularly valuable in scenarios where subtle UI changes could significantly impact user satisfaction. By incorporating visual testing into automated testing frameworks, development teams can achieve a comprehensive and holistic approach to quality assurance, ensuring not only the functional correctness but also the visual integrity of their software products [25, 26].

Image registration can be regarded as a similar computer vision task to change detection; they are two distinct yet interconnected processes. Image registration refers to overlaying two or more images of the same scene or object taken at different times, from different viewpoints, and/or by different sensors [27]. Majority of image registration methods work based on geometrically aligning two images, i.e. the reference (or target) and sensed (or registered) images. The resulting anatomical correspondences between the reference and sensed images allow comparison for down-stream applications [28]. Image registration is a main task in computer vision that has various applications in remote sensing, environmental monitoring, medical image analysis, change detection, weather forecasting, cartography, and other domains [27, 29-35].

On the other hand, visual change detection centres on identifying differences between two images, highlighting alterations in content, structure, or appearance [36, 37]. While image registration establishes correspondences between images, visual change detection identifies regions or features where these correspondences deviate. Despite their differences, there are commonalities between image registration and visual change detection, particularly in their reliance on feature extraction, image matching, and spatial transformations. Both fields benefit from advancements in ML, enabling more robust and automated techniques for registration and change detection [38].

While most of registration methods rely on colour-intensity information or image features such as points, lines, edges, contours, and regions [39-41], features must be extracted from contextual information in change detection, i.e. UI elements in the context of software screenshots. Pixel intensities, lines, and edges cannot usually provide useful information for context-aware modelling of UI layout. In this regard, we use visual and textual similarity between UI elements, as well as, spatial information and similarity between neighbours of a UI control to find correspondence between controls and discover changes.

Deep Learning (DL) techniques have been widely utilized for computer vision tasks, such as image registration [39]. DL models are able to learn higher levels of abstraction in a given problem by learning and combining lower level concepts through a layered processing architecture. They are able to automatically learn features from images. Convolutional Neural Network (CNN) is the most widely used DL architecture for image registration applications [41].

In this work, we utilize YOLO [8], which is a CNN-based object detection model [42], and fine-tune it for the control detection task from software screenshots. UI controls detected by YOLO are used to build a graph model that captures various aspects of the UI layout and context.

Graph-based modelling have applications in various types of image registration methods, e.g. feature-based, intensity-based, and deformable registration [43]. Different graph-based registration methods use various types of information to measure the alignment between images. Entropy and the Jensen-Renyi divergence [44], image structural features [45], and intermediate templates [46] are among sources of information used for graph-based registration. However, these classes of image colour and structural features may not be enough for context-aware visual change detection. To address this challenge, we leverage textual and visual context along with spatial and graph-neighbourhood information to discover deviation in UI layout.

3. Graph-based visual change detection method

Our image change detection model consists of four main steps, i.e. 1) control detection, 2) graph building, 3) graph matching (or graph comparison), 4) and change detection and visualization. We give a detailed description of every step in the following subsections. Figure 1 illustrates the overall architecture of the image change detection method.

Given a target image I and its changed version I' , the problem is to find coordinates within the images where a change has happened and there is a difference between I and I' in those locations. The detected changes are finally visualized using heatmaps H and H' , which show where the changes happen within images I and I' .

3.1. Control detection

In the first step, user interface controls are detected within the images, i.e. the target and changed images. For this purpose, we utilize an object detection machine learning model, i.e. YOLO [8], specifically trained and tested on a user interface control detection dataset containing 14,155 training and 2,000 test samples. The dataset consists of screenshots taken from software applications' windows and annotations of coordinates of controls within images. Every annotated object belongs to one of twenty four classes specifying the type of user interface controls. YOLO is a one-stage object detector; it detects regions of interest and selects the best candidates containing instances of an object of interest end-to-end in one stage. Although the performance of the YOLO object detection model was already discussed on the user interface control detection task in previous work [47], we report the accuracy scores obtained by the model in Table 1, since

the performance of the object detector can directly affect the output of the whole image registration method.

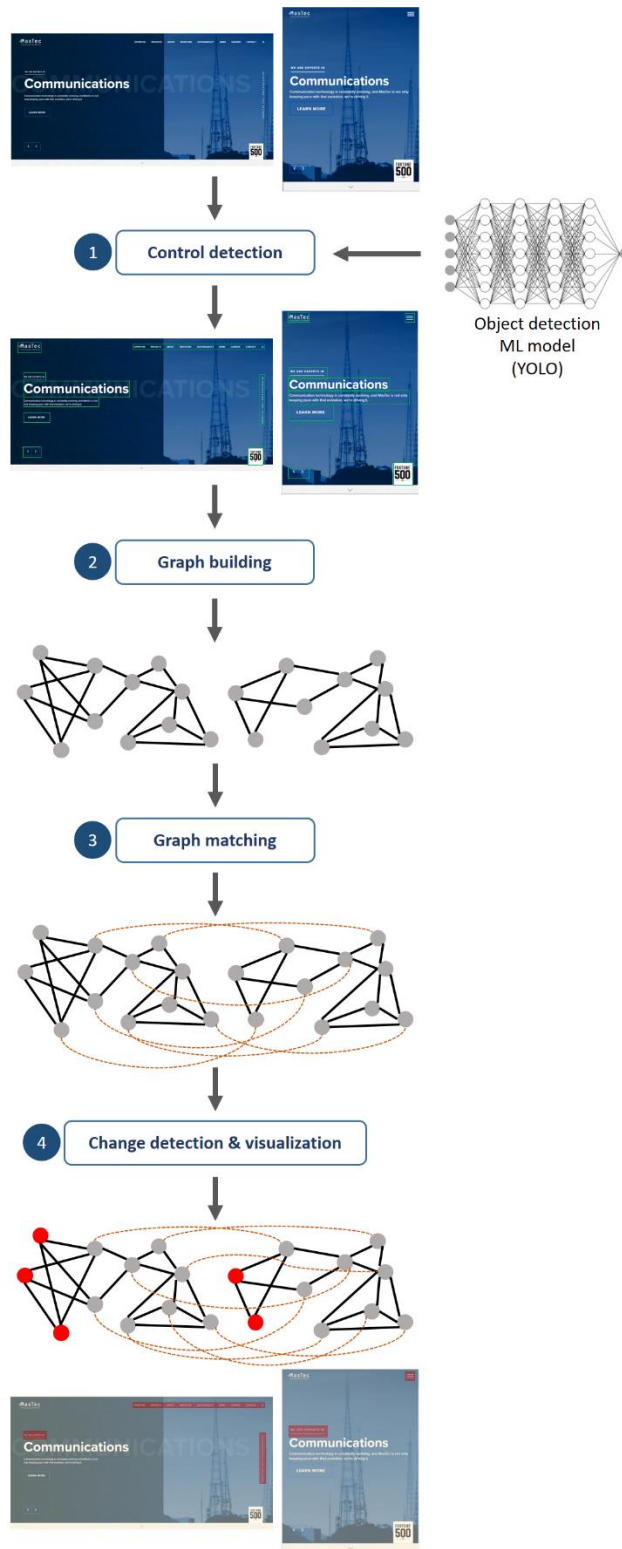


Figure 1. The overall architecture of our graph-based change detection method.

Table 1. Performance scores obtained by the YOLO object detection model on the user interface control detection test set. The YOLO model is used in the first step of our image registration method to detect user interface controls that appear in the software application screenshot images.

Class	Precision	Recall	mAP@.5	mAP@.95
ALL	0.844	0.732	0.735	0.559
ICON	0.948	0.877	0.915	0.63
DROPDOWN	0.884	0.848	0.878	0.681
BUTTON	0.888	0.9	0.917	0.777
MENU	0.876	0.843	0.863	0.655
INPUT	0.909	0.944	0.955	0.797
LIST	0.754	0.679	0.702	0.517
TABBAR	0.827	0.94	0.924	0.768
TABLE	0.823	0.938	0.916	0.782
RADIO_SELECTED	0.923	0.87	0.919	0.644
RADIO_UNSELECTED	0.853	0.919	0.873	0.642
CHECKBOX_UNCHECKED	0.919	0.856	0.857	0.592
CHECKBOX_CHECKED	0.54	0.789	0.659	0.42
TREE	0.771	0.816	0.816	0.639
IMAGE	0.926	0.94	0.934	0.794
TEXT	0.93	0.883	0.932	0.672
LABEL_OF_TEXT_AREA	0.938	0.786	0.88	0.632
DESCRIPTION_LIST	0.817	0.769	0.785	0.645
LEGEND	0.904	0.694	0.773	0.572
HORIZONTAL_AXIS	0.747	0.784	0.81	0.54
CHART	0.911	0.938	0.922	0.793
PLOT_TITLE	0.777	0.944	0.859	0.597
GRAPH	0.766	0.9	0.876	0.671
VERTICAL_AXIS	0.631	0.311	0.309	0.218
DATE_AREA	0.532	0.588	0.572	0.415

The inputs of this step are the target and changed images I and I' , and the outputs are a set of controls $C=\{c_1, c_2, \dots, c_N\}$ detected within image I , another set of controls $C'=\{c'_1, c'_2, \dots, c'_M\}$ detected within image I' , a set of labels $L=\{l_1, l_2, \dots, l_N\}$ such that l_n is the class label assigned to control c_n , and another set of labels $L'=\{l'_1, l'_2, \dots, l'_M\}$ such that l'_m is the class label assigned to control c'_m .

3.2. Graph building

In the second step, an unweighted, undirected graph is built to represent the relationship between the user interface controls within each one of the images. User interface controls detected in the previous step form nodes of the graph. In order to draw edges between the nodes, the Euclidean distance is computed for every pair of nodes, then edges are formed to connect every node to its top K nearest neighbors within the image.

Given a set of controls $C=\{c_1, c_2, \dots, c_N\}$ such that every control is represented as coordinates (x_1, y_1, x_2, y_2) in a two-dimensional space, a list of top K nearest neighbors $NG_n=\{c_1, c_2, \dots, c_K\}$ is created for every c_n . The distance between two controls c_n and c_j is computed using the Euclidean distance as follows:

$$Distance(c_n, c_j) = \sqrt{(x_1 - x'_1)^2 + (y_1 - y'_1)^2 + (x_2 - x'_2)^2 + (y_2 - y'_2)^2} \quad (1)$$

where (x_1, y_1, x_2, y_2) and (x'_1, y'_1, x'_2, y'_2) represent the coordinates of controls c_n and c_j , respectively, within image I .

Algorithm 1 gives the pseudo code of the procedure for creating a list of top K nearest neighbors for every control within the image. For every control, first, an empty list of neighbors is created (lines 3-4). Second, the distance between target control c_n and every other control c_j is computed (lines 5-6). Control c_j is added to the list of nearest neighbors NG_n if the size of the list is still smaller than K (lines 7-8), otherwise, c_j is compared to every $c_p \in NG_n$. Control c_p is removed from NG_n and c_j is added to NG_n if c_j is closer than c_p to target control c_n (lines 9-11). Finally, a list of top K nearest neighbors is returned for every control c_n (line 13).

The same process is also performed for every control c'_m in C' , in order to create a list of top K nearest neighbors $NG'_m=\{c'_1, c'_2, \dots, c'_K\}$ for every control within the changed image.

Algorithm 1. The procedure for creating a list of top K nearest neighbors for controls detected within an image.

```

1: Input: list of detected controls  $C=\{c_1, c_2, \dots, c_N\}$  within image  $I$ , number of top nearest
   neighbors  $K$ 
2: Output: list of top  $K$  nearest neighbor controls  $NG_n=\{c_1, c_2, \dots, c_K\}$  for every control  $c_n$ 
3: for every control  $c_n \in C$ :
4:    $NG_n=\{\}$ 
5:   for every other control  $c_j \in C$ :
6:     compute the distance between  $c_n$  and  $c_j$  using Eq. (1)
7:     if size of  $NG_n$  is smaller than  $K$ :
8:       then add  $c_j$  to  $NG_n$ 
9:     else:
10:      if there is any  $c_p \in NG_n$  where  $Distance(c_n, c_j)$  is greater than  $Distance(c_n, c_p)$ :
11:        then remove  $c_p$  from  $NG_n$  and add  $c_j$  to  $NG_n$ 
12:      end for
13:   return  $NG_n$ 
14: end for

```

After finding the nearest neighbors for every control, a graph $G=(V, E)$ is built to represent how controls in image I are structured. Graph G is composed of a set of vertexes $V=\{v_1, v_2, \dots, v_N\}$ where v_n corresponds to control c_n , and a set of edges $E=\{e_1, e_2, \dots, e_N\}$ where e_n connects a pair of vertexes in V . A graph $G'=(V', E')$ is also built to represent how controls in image I' are structured. Graph G' is composed of a set of vertexes $V'=\{v'_1, v'_2, \dots, v'_M\}$ where v'_m corresponds to control c'_m , and a set of edges $E'=\{e'_1, e'_2, \dots, e'_M\}$ where e'_m connects a pair of vertexes in V' .

3.3. Graph matching

In this step, graphs G and G' are compared to find differences between the graphs, which eventually results in finding changes in the images. We utilize a recursive algorithm to traverse through graphs G and G' and find correspondence between nodes in the graphs.

The main step in this algorithm is to compare every node in G to every node in G' and compute a similarity score for every pair of nodes that have the same class label assigned in the object detection step. The similarity score is computed between nodes $v_n \in V$ and $v'_m \in V'$ by summing up the similarity scores between all neighbors of v_n and v'_m as follows:

$$Similarity(v_n, v'_m) = \sum_{ng_p \in NG_n \text{ and } ng'_q \in NG'_m} Similarity(ng_p, ng'_q) \quad (2)$$

where NG_n is the set of neighbors of v_n , NG'_m is the set of neighbors of v'_m , ng_p is a neighbor of v_n such that $ng_p \in NG_n$ and $1 \leq p \leq K$, and ng'_q is a neighbor of v'_m such that $ng'_q \in NG'_m$ and $1 \leq q \leq K$.

When computing the similarity between nodes v_n and v'_m , the algorithm recursively traverses through neighbors of the nodes and keeps track of nodes it has already seen and computed a similarity value for them. This process continues until the algorithm sees a node it already traversed through and stored in the list of seen nodes. In this situation, a similarity score is computed between ng_p and ng'_q , such that ng_p or ng'_q was already seen in previous recursions, by estimating text similarity and/or hash difference between the nodes. The computed similarity value is then propagated to the previous recursions to compute the final similarity score between v_n and v'_m . In this case, the similarity score is computed as follows:

$$Similarity(ng_p, ng'_q) = TextSim(ng_p, ng'_q) + \frac{1}{HashDiff(ng_p, ng'_q)} \quad (3)$$

where $TextSim(ng_p, ng'_q)$ is the textual similarity between ng_p and ng'_q , and $HashDiff(ng_p, ng'_q)$ is the normalized hash difference between ng_p and ng'_q .

The textual similarity is a value in the range [0, 1], and it equals zero for those pairs of controls that were not classified as text in the control detection step. The higher the text similarity, the more similar the texts that are compared. The hash difference is computed by subtracting the hash code of pixels within the boundaries of the controls in the image. The value of hash difference is equal or greater than zero, such that higher hash values refer to larger differences between images. In order to avoid the similarity score being severely affected by the hash difference, the hash difference values are normalized to values in the range [0, 1]. Since a smaller hash difference means more similarity between controls, the inverse of hash difference is summed up with the textual similarity in Eq. (3).

After computing similarity scores between nodes in G and G' , the change detection method continues with finding the best match for nodes in the graphs. For every node v_n in V , a set of candidate matches CM_n is created, and all nodes in V' whose similarity scores with v_n are larger than threshold $sim_threshold$ are added to CM_n . Finally, the candidate matches are sorted and a node with the highest similarity score is selected as the best match for v_n .

Algorithm 2 gives the pseudo code of the procedure for computing similarity scores and finding the best match for nodes in the graphs. First, nodes in graph G and G' are compared, if they have the same class label, a similarity score is computed using the recursive procedure given

in function *neighbor_sim* (lines 2-6), and a node in G' is added to the target node's list of candidate matches if the similarity score is larger than the threshold (lines 7-8). Then, candidate matches are sorted and a node with the highest similarity score is selected as the best match of the target node. If two or more target nodes share the same node as their best match, the target node having the highest similarity score with the shared node retain it as the best match, and the other target node(s) select a node with the next highest similarity score from their candidate match lists (lines 12-13). The function *neighbor_sim* takes a pair of nodes, their lists of neighbors, and a list of nodes that were already seen in previous recursions of the function (line 15). If both the nodes were not already seen in previous recursions, they are added to the list of nodes that were already seen, and a similarity score is computed by calling the function again and summing up the similarity values resulted from comparing the neighbors (lines 16-22). If one of the nodes were already seen in previous recursions, the similarity is computed by comparing text similarity and/or hash difference between the corresponding controls (lines 23-24).

3.4. Change detection and visualization

After performing the graph matching step, those nodes in G and G' that are similar enough, in terms of similarity between their neighbors (and text similarity and hash difference as well), are matched together. However, some nodes may not be matched with any nodes in the other graph. In this case, controls that correspond to these nodes are detected as changes within the images, because no similar controls with similar neighbors were found.

The visualization is done using heatmaps H and H' , which show where in images I and I' there are differences and something has changed. Heatmaps H and H' are two-dimensional matrices with the same width and height as images I and I' , respectively, and zero as the initial value of all the elements. If no matching node is found for node v_n , the change detection model considers the corresponding control c_n as a control in image I that has changed and no longer appears in I' as it appears in I . Therefore, the value of elements in H in the same location as c_n is set to one. Moreover, if no matching node is found for node v'_m , the change detection model considers the corresponding control c'_m as a control in image I' that has changed and no longer appears in I as it appears in I' . In this way, the value of elements in H' in the same location as c'_m is set to one. We present examples of detected changes within images from different datasets in Section 4.5.

Algorithm 2. The procedure for computing similarity scores and finding the best match for nodes in the graphs.

```

1: Input: set of controls  $C=\{c_1, c_2, \dots, c_N\}$  detected within reference image  $I$ , graph  $G=(V, E)$ 
   that represents the structure of controls in  $C$  within  $I$ , set of controls  $C'=\{c'_1, c'_2, \dots, c'_M\}$ 
   detected within changed image  $I'$ , graph  $G'=(V', E')$  that represents the structure of controls in
    $C'$  within  $I'$ , neighbor similarity threshold  $sim\_threshold$ 
2: Output: best matches between nodes in  $V$  and  $V'$ 
3: for every node  $v_n \in V$ :
4:   for every node  $v'_m \in V'$ :
5:     if  $v_n$  and  $v'_m$  have the same class label:
6:       then compute the similarity between  $v_n$  and  $v'_m$  using function  $neighbor\_sim()$ 
7:       if the similarity is larger than  $sim\_threshold$ :
8:         then add  $v'_m$  to list of candidate matches  $CM_n$ 
9:       end for
10:    sort  $CM_n$  and select the node with the highest similarity score as the best match for  $v_n$ 
11:  end for
12: if two or more nodes in  $V$  share the same  $v'_m$  as the best match:
13:   then node  $v_n$  with the highest similarity score remains as the best match with  $v'_m$ , and
   other nodes take a candidate from their  $CM_n$  with the next highest similarity score
14: return a list containing the best match in  $V'$  for every node in  $V$ 
15: function  $neighbor\_sim(v_n, NG_n, v'_m, NG'_m, already\_seen\_list)$ :
16:   if  $v_n$  and  $v'_m$  are not in  $already\_seen\_list$  then:
17:      $temp\_similarity = 0$ 
18:     for every  $ng_p \in NG_n$  and  $ng'_q \in NG'_m$ :
19:       add  $ng_p$  and  $ng'_q$  to  $already\_seen\_list$ 
20:        $temp\_similarity = temp\_similarity + neighbor\_sim(ng_p, NG_p, ng'_q, NG'_q,$ 
 $already\_seen\_list)$  //Equation (2)
21:     end for
22:     return  $temp\_similarity$ 
23:   else if  $v_n$  or  $v'_m$  are in  $already\_seen\_list$  then:
24:     return similarity between  $v_n$  and  $v'_m$  using Equation (3)

```

4. Experimental results

We conducted a set of experiments to investigate the performance of our graph-based change detection method on datasets of web applications images.

4.1. Datasets

We created three different datasets in order to test the performance of our graph-based change detection method in various scenarios. Two datasets were created for change detection within desktop images in two different scenarios. One dataset were created to detect changes between desktop and mobile images.

4.1.1. Desktop screenshots

We collected an initial set of images of 250 websites by taking screenshots of the desktop browser in the maximized mode with a screen size of 1,920 by 1,080 pixels. The first dataset was created by applying eight different types of changes to the initial set of images. A maximum of four changes were applied to every image. The number of changes and the type of changes were selected in a random manner. These are the eight change types:

1) **ADD CONTROL**: It adds a new control to the image in a location where there is no overlap with existing controls.

2) **CHANGE LOCATION**: It removes a control from its original location and puts it in a new location within the image where there is no overlap with other controls.

3) **CHANGE COLOR**: It changes the color of pixels within a control in the image. Those pixels that share the same color take the same new color. In this way, the same texts or shapes that appear in the original control still appear in the changed control but in a different color.

4) **DUPLICATE**: It creates a copy of a control and puts it in the image in a location where there is no overlap with other controls.

5) **REMOVE**: It selects a control and removes it from the image. The location where the deleted control appeared in the original image is filled with the color of pixels in the neighborhood of that area.

6) **RESIZE SMALLER**: it resizes a control and makes it smaller by a ratio between 0.3 and 0.8. The area that was a part of the resized control within the original image and no longer belongs to the resized control within the new image (because the control has been resized and occupies less space) is filled with the color of pixels in the neighborhood.

7) **RESIZE LARGER**: it resizes a control and makes it larger by a ratio between 0.3 and 0.8 if the resized control has no overlap with other controls within the image.

8) **SWAP CONTROLS**: it selects two controls and swaps their locations if they have no overlap with other controls in the new locations within the image.

Seven changed versions were generated for every image in the dataset by applying different change methods. Therefore, the first dataset contains a total number of 1,750 image pairs, every pair is represented by an original image and a corresponding changed image. Annotations were also generated to specify the location of changes for testing the accuracy.

4.1.2. Desktop screenshots–cut images

We created the second dataset to increase the difficulty of detecting changes and evaluate the accuracy of the visual change detection method in a more complicated scenario. We again generated changed images by applying the eight change methods we introduced in Section 3.1.1, but we also cut a region of every image and shifted the remaining part to the center. In this way, some user interface controls no longer appear in the changed image. Moreover, controls in the changed image do not appear in the same coordinates as in the target (or original) image.

This dataset simulates those scenarios where the active window of the application under test is resized and some controls may not appear anymore in the screenshot. Furthermore, the user interface controls do not appear in the same coordinates as the original screenshot taken before resizing the window. Detecting changes in this scenario can be very challenging, because pixel by pixel comparison easily fails in finding correspondence between controls in the target and changed images.

We created this dataset by applying a maximum of four changes (introduced in the previous subsection) to every original screenshot and then cutting a random area of the image in left, right, top, or bottom. The number of changes per image and the type of changes were selected in a random manner. The location of the area that must be cut was selected randomly from the set (left, right, top, bottom), and the number of pixels to cut was also selected randomly from the set (100, 200, 300, 400, 500). Seven changed versions were generated for every image in the dataset by applying different change methods. Therefore, the second dataset contains a total number of 1,750 images, every pair is represented by an original image and a corresponding changed image. Annotations were also generated to specify the location of changes for testing the accuracy.

4.1.3. Desktop–mobile screenshots

The goal of the third dataset is to evaluate the performance of the visual change detection method in detecting differences between screenshots of an application under test in different platforms. We created this dataset by taking screenshots of 180 pairs of different web applications in the desktop and mobile platforms. The size of images is 1,920 by 1,080 pixels in desktop and 576 by 832 pixels in mobile platform. We also generated ground-truth annotations for every pair of desktop and mobile screenshots by manually annotating user interface controls and correspondence between the controls in the images.

4.2. Evaluation metrics

In order to objectively evaluate the performance of our visual change detection method, we used three evaluation measures, i.e. precision, recall, and F-score. Precision, also known as specificity, is an important metric in assessing the accuracy of ML systems. In the context of visual change detection, precision is defined as the ratio of correctly identified changed UI controls to the total number of controls identified by the ML system as changed. The precision score provides insights into the method's ability to minimize false positives, and is calculated as follows:

$$Precision = \frac{True\ positives}{True\ positives + False\ positives} \quad (4)$$

Recall, also known as sensitivity, is another fundamental metric for evaluating the performance of ML systems. In the context of our work, recall measures the ratio of correctly identified changed UI controls to the total number of ground truth changed controls. A high recall score indicates the method's effectiveness in capturing actual changes. The recall is calculated using the following formula:

$$Recall = \frac{True\ positives}{True\ positives + False\ negatives} \quad (5)$$

The F-score, or F-measure, provides a balance between precision and recall. It is particularly useful when there is a need to weigh both false positives and false negatives. The F-score is the harmonic mean of precision and recall and is computed using the following formula:

$$F\text{-score} = 2 \times \frac{Precision \times Recall}{Precision + Recall} \quad (6)$$

These evaluation measures collectively offer a comprehensive assessment of the visual change detection method's performance on the datasets. Precision focuses on the accuracy of the

identified changes, recall emphasizes the method's ability to capture actual changes, and the F-measure provides a balanced evaluation, considering both precision and recall simultaneously.

We report three versions of these metrics when we discuss the experimental results throughout this section. These three versions are explained in the following:

- **precision@0.75, recall@0.75, and F-score@0.75:** these scores are calculated as presented by Equation (4), (5), and (6), but a detected change by the visual change detection method must have an Intersection Over Union (IOU) greater than or equal to 0.75 in order to be counted as a true positive. These metrics evaluate how accurately the change detector can identify at least 75 percent of every change.
- **precision@0.5, recall@0.5, and F-score@0.5:** these scores are calculated as presented by Equation (4), (5), and (6), but a detected change by the change detection method must have an IOU greater than or equal to 0.5 in order to be counted as a true positive. These metrics evaluate how accurately the change detector can identify at least 50 percent of every change.
- **precision@0.25, recall@0.25, and F-score@0.25:** these scores are calculated as presented by Equation (4), (5), and (6), but a detected change by the change detection method must have an IOU greater than or equal to 0.25 in order to be counted as a true positive. These metrics evaluate how accurately the change detector can identify at least 25 percent of every change.

The IOU measures the overlap between the predicted changed area and the ground truth changed area within an image. In the context of visual change detection, if A_p is the area of the predicted change, A_g is the area of the ground truth change, and A_o is the area of their overlap, then IOU is calculated as follows:

$$IOU = \frac{A_o}{A_p + A_g - A_o} \quad (7)$$

The IOU ranges from 0 to 1, where a value of 0 indicates no overlap, and a value of 1 indicates perfect overlap between the predicted and ground changed areas.

4.3. Hyperparameter tuning

As explained in Section 3, our visual change detection method has four hyperparameters that control how the method creates a graph, identifies correspondence between UI controls within images, and detects changes. We designed and conducted a set of experiments to investigate the impact of these hyperparameters on the performance of change detection. In this subsection, we

present and discuss the experimental results obtained by testing different values of the hyperparameters on each of the three datasets. We used 70 percent of each dataset for tuning the hyperparameters and the remaining 30 percent for testing the change detection method against baseline change detectors.

4.3.1. Desktop screenshots

Table 2 presents the performance scores obtained by our graph-based change detection method in the hyperparameter tuning experiments for different values of the parameter K , which specifies the number of top nearest nodes that form neighbors of a node in the graph.

As the results shows, there is a negligible change in precision when K takes different values, but recall considerably changes with different values of this hyperparameter. As can be seen, the method obtained the highest recall and f-score when eight neighbors were used for every node to create the graphs. The recall scores suggest that when few numbers of neighbors (e.g. one, two, or three) are used to create the graph, the change detector may suffer from lack of enough information about the contextual similarity between nodes in the graphs. On the other hand, large numbers of neighbors (e.g. more than eight) may mislead the object detector by providing irrelevant information about contextual similarity between nodes.

Table 2. Performance scores obtained by our graph-based visual change detection method on the desktop screenshots dataset in the hyperparameter tuning experiments. The highest score in each column is shown in underlined face. In this table, results are only reported for different values of the parameter K (the number of top nearest neighbors for each node to build the graph). The other hyperparameters took their best values reported in Table 3, 4, and 5. ($H=10$, $TS=0.7$, $NS=0.8$)

K	@0.75			@0.5			@0.25		
	Precision	Recall	F-score	Precision	Recall	F-score	Precision	Recall	F-score
1	<u>0.853</u>	0.833	0.842	0.884	0.848	0.865	0.918	0.862	0.889
2	0.851	0.841	0.845	0.884	0.867	0.875	0.919	0.885	0.901
3	0.851	0.862	0.856	0.884	0.885	0.884	0.919	0.896	0.907
4	0.848	0.870	0.858	0.880	0.894	0.886	0.914	0.907	0.910
5	0.850	0.886	0.867	0.883	0.909	0.895	0.918	0.922	0.919
6	0.850	0.892	0.870	<u>0.884</u>	0.918	0.900	<u>0.919</u>	0.930	0.924
7	0.848	0.899	0.872	0.883	0.925	0.903	0.917	0.941	0.928
8	0.848	<u>0.913</u>	<u>0.879</u>	0.883	<u>0.929</u>	<u>0.905</u>	0.917	<u>0.947</u>	<u>0.931</u>
9	0.847	0.904	0.874	0.881	0.910	0.895	0.916	0.931	0.923
10	0.849	0.885	0.866	0.883	0.903	0.892	0.918	0.922	0.919

Table 3 presents the performance scores obtained by our change detection method in the hyperparameter tuning experiments for different values of the parameter H , which specifies the maximum hash difference between controls when finding correspondence between them.

As Table 3 shows, precision is not substantially affected by different values of H , but recall can considerably decrease when H takes higher values. This suggests that higher values of this hyperparameter do not provide the change detection method with enough accurate information about the visual similarity between controls, therefore, the method is misled and cannot detect some changes.

Table 3. Performance scores obtained by our graph-based visual change detection method on the desktop screenshots dataset in the hyperparameter tuning experiments. The highest score in each column is shown in underlined face. In this table, results are only reported for different values of the parameter H (the maximum hash difference between controls). The other hyperparameters took their best values reported in Table 2, 4, and 5. ($K=8$, $TS=0.7$, $NS=0.8$)

H	@0.75			@0.5			@0.25		
	Precision	Recall	F-score	Precision	Recall	F-score	Precision	Recall	F-score
5	0.849	0.899	0.873	0.882	0.903	0.892	0.915	0.922	0.918
10	0.848	<u>0.913</u>	<u>0.879</u>	0.883	<u>0.929</u>	<u>0.905</u>	0.917	<u>0.947</u>	<u>0.931</u>
15	0.846	0.884	0.864	0.877	0.898	0.887	0.911	0.920	0.915
20	0.852	0.863	0.857	0.883	0.885	0.883	0.917	0.908	0.912
25	0.850	0.856	0.852	0.879	0.874	0.876	0.915	0.898	0.906
30	0.849	0.833	0.840	0.879	0.852	0.865	0.914	0.876	0.894
35	0.857	0.808	0.831	0.886	0.836	0.860	<u>0.920</u>	0.847	0.881
40	<u>0.858</u>	0.794	0.824	<u>0.887</u>	0.823	0.853	0.920	0.832	0.873

Table 4 presents the performance scores obtained by our change detection method in the hyperparameter tuning experiments for different values of the parameter TS , which specifies the minimum text similarity between controls when finding correspondence between them.

As the results show, both precision and recall are affected by changing the value of TS , however, the latter is influenced by a higher degree. The change detector showed its best performance when the minimum textual similarity was set to 0.8. The results demonstrate that smaller textual similarity thresholds mislead the method by allowing dissimilar controls to be identified as corresponding nodes between the graphs. Higher values of TS can be also misleading by preventing small degrees of deviation in the textual content of corresponding controls.

Table 5 presents the performance scores obtained by our change detection method in the hyperparameter tuning experiments for different values of the parameter NS , which specifies the minimum neighbor similarity between nodes in graphs when finding similar nodes. As reported in Table 5, different values of NS can considerably affect the recall scores. The highest scores were obtained when the minimum neighbor similarity threshold was 0.8, however, smaller values reduced the change detector’s performance. This suggests that smaller neighbor similarity thresholds lead to establishing wrong correspondence between controls, because it allows some nodes that do not have enough similar neighbors to be identified as analogous. As a result, the change detection method cannot be able to accurately identify all the corresponding controls, therefore, some changes are not detected.

Table 4. Performance scores obtained by our graph-based visual change detection method on the desktop screenshots dataset in the hyperparameter tuning experiments. The highest score in each column is shown in underlined face. In this table, results are only reported for different values of the parameter TS (the minimum text similarity between controls that belong to the class TEXT). The other hyperparameters took their best values reported in Table 2, 3, and 5. ($K=8, H=10, NS=0.8$)

TS	<u>@0.75</u>			<u>@0.5</u>			<u>@0.25</u>		
	Precision	Recall	F-score	Precision	Recall	F-score	Precision	Recall	F-score
0.1	0.817	0.819	0.818	0.848	0.840	0.844	0.861	0.886	0.873
0.2	0.821	0.831	0.825	0.854	0.855	0.854	0.870	0.898	0.883
0.3	0.825	0.848	0.836	0.859	0.862	0.860	0.875	0.911	0.892
0.4	0.834	0.860	0.846	0.871	0.877	0.873	0.899	0.918	0.908
0.5	0.834	0.882	0.857	0.871	0.897	0.883	0.899	0.924	0.911
0.6	0.839	0.902	0.869	0.875	0.916	0.895	0.904	0.933	0.918
0.7	<u>0.848</u>	<u>0.913</u>	<u>0.879</u>	<u>0.883</u>	<u>0.929</u>	<u>0.905</u>	<u>0.917</u>	<u>0.947</u>	<u>0.931</u>
0.8	0.848	0.905	0.875	0.883	0.918	0.900	0.917	0.938	0.927
0.9	0.837	0.891	0.863	0.871	0.906	0.888	0.906	0.931	0.918

4.3.2. Desktop screenshots–cut images

In this subsection, we present the hyperparameter tuning results on the desktop screenshots–cut images dataset. Table 6, 7, 8, and 9 give the performance scores obtained by our graph-based change detector for different values of the parameters K , H , TS , and NS , respectively.

The results show almost the same patterns we discussed in Section 3.3.1 for the hyperparameter tuning experiments on the desktop screenshots dataset. However, the best results are reported for $K=6$ when experimenting with different values on the desktop screenshots–cut

images dataset. The reason may be that some regions of the changed images were cut in this dataset, hence, some controls missed their closer neighbors in the UI. These controls were consequently connected to farther neighbors in the graph due to a larger value of K , e.g. eight. Being connected to farther neighbors in the graph created for the changed image can cause the change detection model being misled in finding proper correspondence between controls, since the corresponding control in the original image is still connected to the closer neighbors in the graph. Therefore, a smaller value of K , e.g. six, can help the method to perform more accurately in detecting changes by considering fewer neighbors in the graph in scenarios where not all the original UI controls are visible in the changed image (for instance, when the application window has been resized, or some part of it is covered by other windows).

Table 5. Performance scores obtained by our graph-based visual change detection method on the desktop screenshots dataset in the hyperparameter tuning experiments. The highest score in each column is shown in underlined face. In this table, results are only reported for different values of the parameter NS (the minimum neighbor similarity between nodes in the graph when identifying similar nodes). The other hyperparameters took their best values reported in Table 2, 3, and 4. ($K=8, H=10, TS=0.7$)

NS	@0.75			@0.5			@0.25		
	Precision	Recall	F-score	Precision	Recall	F-score	Precision	Recall	F-score
0.1	0.864	0.831	0.847	0.896	0.852	0.873	0.928	0.848	0.886
0.2	<u>0.864</u>	0.832	0.847	<u>0.896</u>	0.853	0.873	0.928	0.869	0.897
0.3	0.860	0.856	0.857	0.892	0.877	0.884	0.927	0.886	0.906
0.4	0.861	0.856	0.858	0.893	0.877	0.884	0.928	0.885	0.905
0.5	0.861	0.856	0.858	0.893	0.877	0.884	<u>0.928</u>	0.885	0.905
0.6	0.854	0.876	0.864	0.886	0.897	0.891	0.921	0.907	0.913
0.7	0.854	0.876	0.864	0.886	0.897	0.891	0.921	0.907	0.913
0.8	0.848	<u>0.913</u>	<u>0.879</u>	0.883	<u>0.929</u>	<u>0.905</u>	0.917	<u>0.947</u>	<u>0.931</u>
0.9	0.848	0.906	0.876	0.880	0.918	0.898	0.915	0.929	0.921

Table 6. Performance scores obtained by our graph-based visual change detection method on the desktop screenshots–cut images dataset in the hyperparameter tuning experiments. The highest score in each column is shown in underlined face. In this table, results are only reported for different values of the parameter K (the number of top nearest neighbors for each node to build the graph). The other hyperparameters took their best values reported in Table 7, 8, and 9. ($H=10$, $TS=0.7$, $NS=0.8$)

K	@0.75			@0.5			@0.25		
	Precision	Recall	F-score	Precision	Recall	F-score	Precision	Recall	F-score
1	0.824	0.801	0.812	0.851	0.815	0.832	0.882	0.830	0.855
2	0.826	0.813	0.819	0.855	0.832	0.843	0.878	0.854	0.865
3	0.824	0.830	0.826	0.855	0.851	0.852	0.885	0.861	0.872
4	0.817	0.838	0.827	0.851	0.859	0.854	0.873	0.872	0.872
5	0.826	0.849	0.837	0.847	0.878	0.862	0.882	0.879	0.880
6	<u>0.829</u>	<u>0.862</u>	<u>0.845</u>	<u>0.855</u>	<u>0.895</u>	<u>0.874</u>	<u>0.889</u>	<u>0.905</u>	<u>0.896</u>
7	0.817	0.858	0.836	0.851	0.883	0.866	0.885	0.901	0.892
8	0.815	0.855	0.834	0.845	0.887	0.865	0.875	0.905	0.889
9	0.815	0.838	0.826	0.849	0.865	0.856	0.871	0.892	0.881
10	0.824	0.830	0.826	0.851	0.850	0.850	0.878	0.887	0.882

Table 7. Performance scores obtained by our graph-based visual change detection method on the desktop screenshots–cut images dataset in the hyperparameter tuning experiments. The highest score in each column is shown in underlined face. In this table, results are only reported for different values of the parameter H (the maximum hash difference between controls). The other hyperparameters took their best values reported in Table 6, 8, and 9. ($K=6$, $TS=0.7$, $NS=0.8$)

H	@0.75			@0.5			@0.25		
	Precision	Recall	F-score	Precision	Recall	F-score	Precision	Recall	F-score
5	0.822	0.850	0.835	0.848	0.881	0.864	0.871	0.894	0.882
10	0.829	<u>0.862</u>	<u>0.845</u>	0.855	<u>0.895</u>	<u>0.874</u>	0.889	<u>0.905</u>	<u>0.896</u>
15	0.825	0.839	0.831	0.850	0.863	0.856	0.876	0.879	0.877
20	<u>0.834</u>	0.821	0.827	<u>0.859</u>	0.847	0.852	<u>0.894</u>	0.862	0.877
25	0.829	0.813	0.820	0.855	0.836	0.845	0.889	0.850	0.869
30	0.822	0.803	0.812	0.848	0.825	0.836	0.871	0.837	0.853
35	0.817	0.785	0.800	0.842	0.809	0.825	0.868	0.815	0.840
40	0.829	0.754	0.789	0.855	0.782	0.816	0.871	0.796	0.831

Table 8. Performance scores obtained by our graph-based visual change detection method on the desktop screenshots–cut images dataset in the hyperparameter tuning experiments. The highest score in each column is shown in underlined face. In this table, results are only reported for different values of the parameter TS (the minimum text similarity between controls that belong to the class TEXT). The other hyperparameters took their best values reported in Table 6, 7, and 9. ($K=6, H=10, NS=0.8$)

TS	<u>@0.75</u>			<u>@0.5</u>			<u>@0.25</u>		
	Precision	Recall	F-score	Precision	Recall	F-score	Precision	Recall	F-score
0.1	0.787	0.772	0.779	0.817	0.807	0.811	0.846	0.815	0.830
0.2	0.796	0.784	0.789	0.823	0.816	0.819	0.855	0.829	0.841
0.3	0.805	0.797	0.800	0.828	0.831	0.829	0.858	0.857	0.857
0.4	0.813	0.821	0.816	0.837	0.854	0.845	0.862	0.872	0.866
0.5	0.817	0.839	0.827	0.842	0.866	0.853	0.871	0.879	0.874
0.6	0.822	0.854	0.837	0.848	0.885	0.866	0.877	0.899	0.887
0.7	0.829	<u>0.862</u>	<u>0.845</u>	0.855	<u>0.895</u>	<u>0.874</u>	0.889	<u>0.905</u>	<u>0.896</u>
0.8	<u>0.834</u>	0.847	0.840	<u>0.862</u>	0.873	0.867	<u>0.897</u>	0.888	0.892
0.9	0.822	0.839	0.830	0.848	0.862	0.854	0.868	0.873	0.870

Table 9. Performance scores obtained by our graph-based visual change detection method on the desktop screenshots–cut images dataset in the hyperparameter tuning experiments. The highest score in each column is shown in underlined face. In this table, results are only reported for different values of the parameter NS (the minimum neighbor similarity between nodes in the graph when identifying similar nodes). The other hyperparameters took their best values reported in Table 6, 7, and 8. ($K=6, H=10, TS=0.7$)

NS	<u>@0.75</u>			<u>@0.5</u>			<u>@0.25</u>		
	Precision	Recall	F-score	Precision	Recall	F-score	Precision	Recall	F-score
0.1	0.838	0.786	0.811	0.865	0.811	0.837	0.899	0.826	0.860
0.2	0.838	0.786	0.811	0.865	0.811	0.837	0.905	0.826	0.863
0.3	<u>0.848</u>	0.805	0.825	<u>0.879</u>	0.834	0.855	<u>0.912</u>	0.845	0.877
0.4	0.842	0.817	0.829	0.871	0.847	0.858	0.905	0.861	0.882
0.5	0.842	0.817	0.829	0.871	0.847	0.858	0.905	0.861	0.882
0.6	0.833	0.834	0.833	0.859	0.865	0.861	0.894	0.868	0.880
0.7	0.833	0.834	0.833	0.859	0.865	0.861	0.894	0.877	0.885
0.8	0.829	<u>0.862</u>	<u>0.845</u>	0.855	<u>0.895</u>	<u>0.874</u>	0.889	<u>0.905</u>	<u>0.896</u>
0.9	0.821	0.853	0.836	0.846	0.883	0.864	0.875	0.892	0.883

4.3.3. Desktop–mobile screenshots

In this subsection, we present the hyperparameter tuning results on the desktop–mobile screenshots dataset. Table 10, 11, 12, and 13 give the performance scores obtained by our graph-based change detector for different values of the parameters K , H , TS , and NS , respectively.

The results show almost the same patterns we discussed in Section 3.3.1 and Section 3.3.2 for the hyperparameter tuning experiments on the other two datasets. However, the best results are reported for $K=5$ when experimenting with different values on the desktop–mobile dataset. The reason can be fewer number of controls and lower control density in the mobile images. When more numbers of neighbors, e.g. eight or nine, are used to create the graph for the mobile image, some neighbors may be too distant from a target node, whereas the same controls may not be connected to the corresponding node in the graph created for the desktop image. As a result, the graph cannot provide the change detector with highly accurate information about the most relevant neighbors of every control. On the other hand, smaller values of the parameter K , e.g. five or six, lead to discarding farther neighbors, which eventually help the change detector identify correspondence between controls with respect to their most relevant neighbors.

Table 10. Performance scores obtained by our graph-based visual change detection method on the desktop–mobile screenshots dataset in the hyperparameter tuning experiments. The highest score in each column is shown in underlined face. In this table, results are only reported for different values of the parameter K (the number of top nearest neighbors for each node to build the graph). The other hyperparameters took their best values reported in Table 11, 12, and 13. ($H=10$, $TS=0.7$, $NS=0.8$)

K	@0.75			@0.5			@0.25		
	Precision	Recall	F-score	Precision	Recall	F-score	Precision	Recall	F-score
1	0.828	0.801	0.814	0.835	0.824	0.829	0.855	0.833	0.843
2	0.839	0.815	0.826	0.844	0.839	0.841	0.872	0.850	0.860
3	0.839	0.820	0.829	0.844	0.847	0.845	0.872	0.862	0.866
4	<u>0.849</u>	0.820	0.834	<u>0.863</u>	0.853	0.857	<u>0.889</u>	0.871	0.879
5	0.835	<u>0.843</u>	<u>0.838</u>	0.852	<u>0.874</u>	<u>0.862</u>	0.881	<u>0.894</u>	<u>0.887</u>
6	0.835	0.836	0.835	0.852	0.862	0.856	0.881	0.879	0.879
7	0.842	0.830	0.835	0.857	0.853	0.854	0.885	0.871	0.877
8	0.835	0.824	0.829	0.852	0.841	0.846	0.881	0.858	0.869
9	0.842	0.811	0.826	0.857	0.837	0.846	0.885	0.846	0.865
10	0.839	0.804	0.821	0.844	0.830	0.836	0.872	0.837	0.854

Table 11. Performance scores obtained by our graph-based visual change detection method on the desktop–mobile screenshots dataset in the hyperparameter tuning experiments. The highest score in each column is shown in underlined face. In this table, results are only reported for different values of the parameter H (the maximum hash difference between controls). The other hyperparameters took their best values reported in Table 10, 12, and 13. ($K=5$, $TS=0.7$, $NS=0.8$)

H	@0.75			@0.5			@0.25		
	Precision	Recall	F-score	Precision	Recall	F-score	Precision	Recall	F-score
5	0.826	0.827	0.826	0.841	0.851	0.845	0.868	0.874	0.870
10	0.835	<u>0.843</u>	<u>0.838</u>	0.852	<u>0.874</u>	<u>0.862</u>	0.881	<u>0.894</u>	<u>0.887</u>
15	0.835	0.831	0.832	0.852	0.865	0.858	0.881	0.877	0.878
20	<u>0.839</u>	0.818	0.828	<u>0.859</u>	0.843	0.850	<u>0.889</u>	0.852	0.870
25	0.822	0.805	0.813	0.836	0.829	0.832	0.862	0.831	0.846
30	0.835	0.796	0.815	0.852	0.817	0.834	0.881	0.829	0.854
35	0.826	0.774	0.799	0.841	0.796	0.817	0.868	0.808	0.836
40	0.826	0.755	0.788	0.841	0.770	0.803	0.868	0.777	0.819

Table 12. Performance scores obtained by our graph-based visual change detection method on the desktop–mobile screenshots dataset in the hyperparameter tuning experiments. The highest score in each column is shown in underlined face. In this table, results are only reported for different values of the parameter TS (the minimum text similarity between controls that belong to the class TEXT). The other hyperparameters took their best values reported in Table 10, 11, and 13. ($K=5$, $H=10$, $NS=0.8$)

TS	@0.75			@0.5			@0.25		
	Precision	Recall	F-score	Precision	Recall	F-score	Precision	Recall	F-score
0.1	0.801	0.752	0.775	0.821	0.780	0.799	0.842	0.802	0.821
0.2	0.806	0.763	0.783	0.827	0.795	0.810	0.847	0.817	0.831
0.3	0.812	0.787	0.799	0.833	0.816	0.824	0.861	0.829	0.844
0.4	0.817	0.799	0.807	0.833	0.827	0.829	0.866	0.845	0.855
0.5	0.829	0.815	0.821	0.840	0.848	0.843	0.872	0.861	0.866
0.6	0.829	0.827	0.827	0.840	0.861	0.850	0.872	0.883	0.877
0.7	0.835	<u>0.843</u>	<u>0.838</u>	0.852	<u>0.874</u>	<u>0.862</u>	0.881	<u>0.894</u>	<u>0.887</u>
0.8	<u>0.841</u>	0.821	0.830	<u>0.863</u>	0.850	0.856	<u>0.889</u>	0.875	0.881
0.9	0.841	0.805	0.822	0.863	0.831	0.846	0.889	0.866	0.877

Table 13. Performance scores obtained by our graph-based visual change detection method on the desktop–mobile screenshots dataset in the hyperparameter tuning experiments. The highest score in each column is shown in underlined face. In this table, results are only reported for different values of the parameter NS (the minimum neighbor similarity between nodes in the graph when identifying similar nodes). The other hyperparameters took their best values reported in Table 10, 11, and 12. ($K=5, H=10, TS=0.7$)

NS	<u>@0.75</u>			<u>@0.5</u>			<u>@0.25</u>		
	Precision	Recall	F-score	Precision	Recall	F-score	Precision	Recall	F-score
0.1	0.820	0.795	0.807	0.838	0.822	0.829	0.865	0.840	0.852
0.2	0.835	0.801	0.817	0.852	0.836	0.843	0.881	0.851	0.865
0.3	0.845	0.817	0.831	0.869	0.841	0.854	0.893	0.858	0.875
0.4	<u>0.845</u>	0.817	0.831	<u>0.869</u>	0.841	0.854	<u>0.893</u>	0.858	0.875
0.5	0.841	0.820	0.830	0.864	0.848	0.855	0.887	0.863	0.874
0.6	0.835	0.826	0.830	0.852	0.855	0.853	0.881	0.870	0.875
0.7	0.826	0.835	0.830	0.843	0.865	0.854	0.870	0.881	0.875
0.8	0.835	<u>0.843</u>	<u>0.838</u>	0.852	<u>0.874</u>	<u>0.862</u>	0.881	<u>0.894</u>	<u>0.887</u>
0.9	0.830	0.830	0.830	0.852	0.862	0.856	0.881	0.875	0.877

4.4. Baselines

We designed and conducted another set of experiments to evaluate the performance of our visual change detection method against other change detectors. Given the innovative nature of our approach, there exists a lack of directly comparable methods in the existing literature. Existing visual change detection tools often rely on pixel-level comparisons, lacking the sophistication necessary for nuanced UI change detection. In the absence of directly analogous methods, we implemented two baseline change detectors to establish a meaningful context for evaluating our proposed method. These baselines are designed to represent conventional strategies for change detection in software interfaces and serve as benchmarks against which the performance of our method can be objectively assessed. We describe these two baselines in the following subsections.

4.4.1. Pixel-wise comparison

This baseline method involves a pixel-wise comparison of the original and modified software screenshots. Pixels in the same location within the original and changed images are compared against each other and that location is marked as a change if the pixel values are different. This approach, although simplistic, reflects a common strategy employed in many visual change detection methodologies. However, it fails to capture the semantic relationships between user interface controls and has limited adaptability to dynamic interface changes.

4.4.2. Region-based change detection

The second baseline method employs a region-based approach, wherein predefined regions of interest, i.e. UI controls, within the software screenshot are analyzed for changes. UI controls are first detected using the YOLO object detection model, then, controls in the same location within the images are compared using the hash difference. Controls are marked as a change if they have a hash difference higher than 10 with their corresponding region within the other image. This hash difference threshold was specified by hyperparameter tuning on the training datasets. While this baseline method introduces a level of abstraction beyond pixel-wise comparison, it may struggle with capturing spatial relationships and nuanced changes that extend beyond control-wise visual similarity.

4.5. Performance evaluation against baselines

Table 14, 15, and 16 present the performance scores obtained by our graph-based visual change detection method and the two baselines on the desktop screenshots, desktop screenshots–cut images, and desktop–mobile screenshots test datasets, respectively.

As Table 14 shows, the pixel-wise comparison (PWC) baseline can perform better than the other methods in the simplest scenario, i.e. detecting UI changes when the original and changed screenshots come from the same modality (desktop UI in this case), with the same size, no resizing, and no cut regions. However, in more complicated scenarios, as can be seen in Table 15 and 16, the pixel-wise comparison fails to properly detect changes.

Our graph-based change detector could not perform better than the pixel-wise comparison baseline on the desktop screenshots dataset. However, it achieved a precision of more than 85 percent and a recall of more than 92 percent. On the other two datasets, our change detection method outperformed the two baselines.

Table 14. Performance scores obtained by our graph-based visual change detection method and the baselines on the desktop screenshots test dataset. The highest score in each column is shown in underlined face. PWC: Pixel-wise Comparison, RCD: Region-based Change Detection, GVCD: our Graph-based Visual Change Detection.

	<u>@0.75</u>			<u>@0.5</u>			<u>@0.25</u>		
	<u>Precision</u>	<u>Recall</u>	<u>F-score</u>	<u>Precision</u>	<u>Recall</u>	<u>F-score</u>	<u>Precision</u>	<u>Recall</u>	<u>F-score</u>
PWC baseline	<u>1.000</u>	<u>0.931</u>	<u>0.964</u>	<u>1.000</u>	<u>0.948</u>	<u>0.973</u>	<u>1.000</u>	<u>0.961</u>	<u>0.980</u>
RCD baseline	0.762	0.775	0.768	0.786	0.802	0.793	0.803	0.819	0.810
GVCD	0.853	0.922	0.886	0.891	0.935	0.912	0.927	0.953	0.939

Table 15. Performance scores obtained by our graph-based visual change detection method and the baselines on the desktop screenshots–cut images test dataset. The highest score in each column is shown in underlined face. PWC: Pixel-wise Comparison, RCD: Region-based Change Detection, GVCD: our Graph-based Visual Change Detection.

	@0.75			@0.5			@0.25		
	Precision	Recall	F-score	Precision	Recall	F-score	Precision	Recall	F-score
PWC baseline	-	-	-	-	-	-	-	-	-
RCD baseline	0.656	0.684	0.669	0.692	0.704	0.697	0.712	0.719	0.715
GVCD	<u>0.835</u>	<u>0.870</u>	<u>0.852</u>	<u>0.862</u>	<u>0.899</u>	<u>0.880</u>	<u>0.897</u>	<u>0.911</u>	<u>0.903</u>

Table 16. Performance scores obtained by our graph-based visual change detection method and the baselines on the desktop–mobile screenshots test dataset. The highest score in each column is shown in underlined face. PWC: Pixel-wise Comparison, RCD: Region-based Change Detection, GVCD: our Graph-based Visual Change Detection.

	@0.75			@0.5			@0.25		
	Precision	Recall	F-score	Precision	Recall	F-score	Precision	Recall	F-score
PWC baseline	-	-	-	-	-	-	-	-	-
RCD baseline	0.620	0.632	0.625	0.651	0.649	0.650	0.673	0.664	0.668
GVCD	<u>0.841</u>	<u>0.849</u>	<u>0.844</u>	<u>0.862</u>	<u>0.880</u>	<u>0.871</u>	<u>0.887</u>	<u>0.905</u>	<u>0.896</u>

Figure 2 shows a pair of images from the desktop screenshots dataset, and heatmaps that show visual changes detected by our graph-based change detection method. As can be seen, all the changes have been accurately detected within this pair of screenshots. The pixel-wise comparison can also perfectly perform on this dataset since the screenshot pairs were exactly taken from the same location in the applications, without resizing the window and cutting some parts of the images. In this simple scenario, it is imperative for change detection methods to exhibit a high degree of precision and recall.

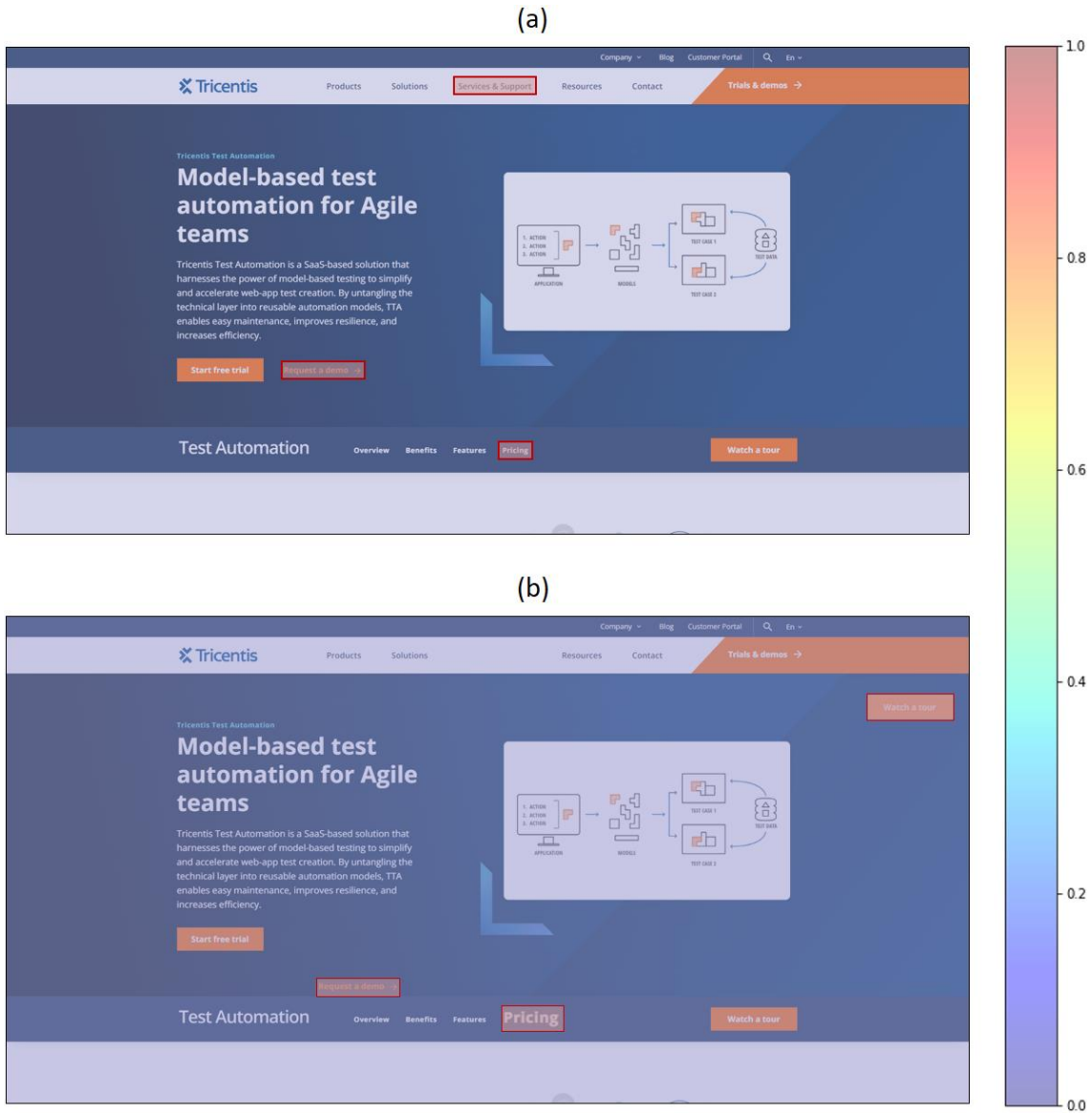


Figure 2. A pair of images from the desktop screenshots dataset, and heatmaps that show visual changes detected by our graph-based change detection method. (a) The original screenshot, (b) the changed screenshot. The changes are shown by red-bordered rectangles.

Figure 3 shows a pair of images from the desktop screenshots–cut images dataset, and heatmaps that show visual changes detected by our graph-based change detection method. As the images show, in this scenario, some part of the image is not visible in the changed version (this simulates resizing the software/application window). Therefore, the UI controls do not appear in the same coordinate within the changed image as the original screenshot. In this case, the pixel-wise comparison totally fails to detect changes because it relies on comparing pixels in the same coordinate between the images. The region-based baseline performs better than the pixel-wise comparison, however, it underperforms the graph-based change detector. The graph model

provides the change detector with a context-aware representation of the UI layout that can effectively identify which UI element deviates from its original context within the target image.

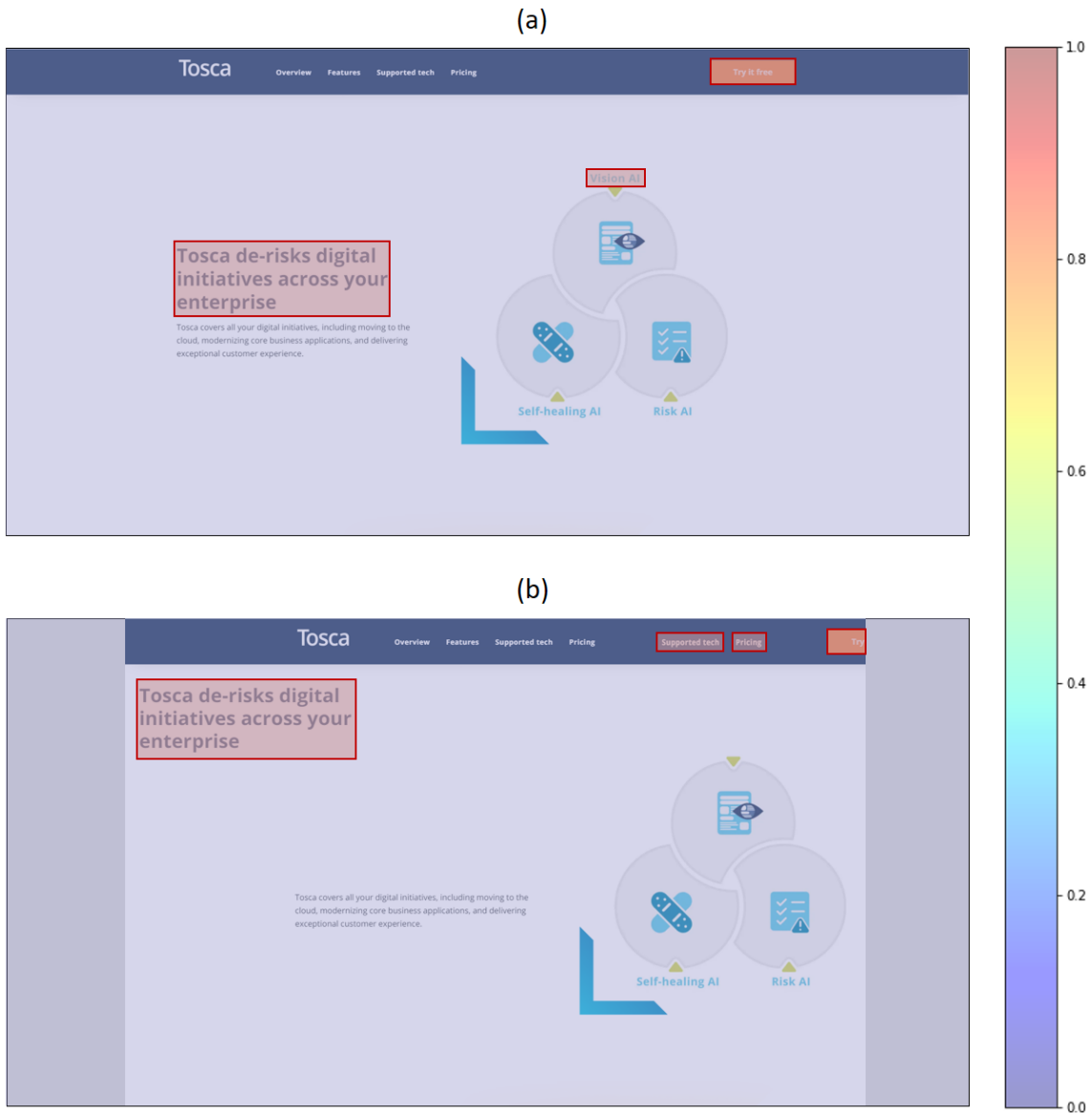


Figure 3. A pair of images from the desktop screenshots–cut images dataset, and heatmaps that show visual changes detected by our graph-based change detection method. (a) The original screenshot, (b) the changed screenshot. The changes are shown by red-bordered rectangles.

Figure 4 shows a pair of images from the desktop–mobile screenshots dataset, and heatmaps that show visual changes detected by our graph-based change detection method. As can be seen, our method has been also able to accurately detect differences between the screenshots of the same application from desktop and mobile platforms. The pixel-wise comparison totally fails in this scenario as well. The region-based baseline performed better than the other baseline, however it still underperforms the graph-based change detector since it suffers from lack of contextual information. These examples of various visual testing scenarios demonstrate the effectiveness of

our change detection model for identifying visual regressions in automated software testing and quality assurance.



Figure 4. A pair of images from the desktop–mobile screenshots dataset, and heatmaps that show visual differences detected by our graph-based change detection method. (a) The original screenshot from desktop platform, (b) the screenshot from mobile platform. The differences are shown by red-bordered rectangles.

5. Conclusion

In this paper, we presented a novel method for visual change detection in software test automation, combining computer vision, ML, and graph-based analysis. Our approach, which involves detecting UI controls, constructing context-aware graph models, and comparing correspondences between the original and changed versions of software screenshots, addresses

the limitations of traditional pixel-wise and region-based techniques. Through extensive experimentation, we demonstrated the method's efficacy in detecting various interface changes and its superiority over baseline methods, particularly in more complex visual testing scenarios. The use of a ML model for control detection and the subsequent graph-based analysis not only enhances the precision of change detection but also provides a contextual understanding of the spatial relationships between controls, as well as their visual and textual content. This holistic representation of the UI contributes to the robustness of our method, allowing it to adapt to diverse simple and complex testing scenarios.

The experimental results underscore the practical significance of our method in enhancing the accuracy, efficiency, and reliability of visual change detection, which plays an integral role in software test automation. As software systems evolve and interface intricacies grow, the presented approach offers a forward-thinking solution to address the challenges associated with dynamic user interfaces. Looking ahead, our work opens avenues for further exploration at the intersection of AI, and software testing methodologies. The proposed method not only contributes to the advancement of automated software testing but also holds promise for future research endeavors, fostering innovation in the dynamic landscape of software development and quality assurance.

Building on the foundational work of utilizing AI for detecting visual changes in software screenshots, future research could focus on several promising avenues. One potential area is the integration of DL techniques to enhance the granularity and accuracy of change detection, enabling the system to identify subtle differences that might affect UX but are currently undetectable with existing methods. Additionally, the development of AI-driven predictive models could foresee possible UI inconsistencies caused by changes in the software environment or updates, allowing developers to proactively adjust designs. Another area for expansion is the application of reinforcement learning to continuously improve test automation processes based on feedback loops from past testing cycles. This could significantly reduce human intervention in UI testing, leading to more efficient and less error-prone software development pipelines. Finally, exploring the intersection of AI with augmented and virtual reality could offer innovative ways to test and ensure the quality of immersive user interfaces, catering to the evolving demands of modern software applications.

Statements and Declarations

The authors have no relevant financial or non-financial interests to disclose. The authors have no conflicts of interest to declare that are relevant to the content of this article.

References

- [1] C. Y. Laporte and A. April, *Software quality assurance*: John Wiley & Sons, 2018.
- [2] K. Naik and P. Tripathy, *Software testing and quality assurance: theory and practice*: John Wiley & Sons, 2011.
- [3] M. Hossain, "Challenges of software quality assurance and testing," *International Journal of Software Engineering and Computer Systems*, vol. 4, pp. 133-144, 2018.
- [4] N. Walkinshaw, "Software quality assurance," *Springer Int Publ*, vol. 10, pp. 978-983, 2017.
- [5] B. R. Maxim and M. Kessentini, "Chapter 2 - An introduction to modern software quality assurance," in *Software Quality Assurance*, I. Mistrik, R. Soley, N. Ali, J. Grundy, and B. Tekinerdogan, Eds., ed Boston: Morgan Kaufmann, 2016, pp. 19-46.
- [6] K. Wiklund, S. Eldh, D. Sundmark, and K. Lundqvist, "Impediments for software test automation: A systematic literature review," *Software Testing, Verification and Reliability*, vol. 27, p. e1639, 2017.
- [7] Y. Wang, M. V. Mäntylä, S. Demeyer, K. Wiklund, S. Eldh, and T. Kairi, "Software Test Automation Maturity--A Survey of the State of the Practice," *arXiv preprint arXiv:2004.09210*, 2020.
- [8] J. Redmon, S. Divvala, R. Girshick, and A. Farhadi, "You only look once: Unified, real-time object detection," in *Proceedings of the IEEE conference on computer vision and pattern recognition*, 2016, pp. 779-788.
- [9] M. A. Jamil, M. Arif, N. S. A. Abubakar, and A. Ahmad, "Software Testing Techniques: A Literature Review," in *2016 6th International Conference on Information and Communication Technology for The Muslim World (ICT4M)*, 2016, pp. 177-182.
- [10] L. Luo, "Software testing techniques," *Institute for software research international Carnegie mellon university Pittsburgh, PA*, vol. 15232, p. 19, 2001.
- [11] A. A. Sawant, P. H. Bari, and P. Chawan, "Software testing techniques and strategies," *International Journal of Engineering Research and Applications (IJERA)*, vol. 2, pp. 980-986, 2012.
- [12] J. Kasurinen, O. Taipale, and K. Smolander, "Software test automation in practice: empirical observations," *Advances in Software Engineering*, vol. 2010, 2010.
- [13] K. Karhu, T. Repo, O. Taipale, and K. Smolander, "Empirical Observations on Software Testing Automation," in *2009 International Conference on Software Testing Verification and Validation*, 2009, pp. 201-209.
- [14] V. Garousi and M. V. Mäntylä, "When and what to automate in software testing? A multi-vocal literature review," *Information and Software Technology*, vol. 76, pp. 92-117, 2016.
- [15] M. A. Umar and C. Zhanfang, "A study of automated software testing: Automation tools and frameworks," *International Journal of Computer Science Engineering (IJCSE)*, vol. 6, pp. 217-225, 2019.
- [16] M. R. Pratama and D. S. Kusumo, "Implementation of Continuous Integration and Continuous Delivery (CI/CD) on Automatic Performance Testing," in *2021 9th International Conference on Information and Communication Technology (ICoICT)*, 2021, pp. 230-235.
- [17] K. Sneha and G. M. Malle, "Research on software testing techniques and software automation testing tools," in *2017 International Conference on Energy, Communication, Data Analytics and Soft Computing (ICECDS)*, 2017, pp. 77-81.
- [18] M. Navaei and N. Tabrizi, "Machine Learning in Software Development Life Cycle: A Comprehensive Review," *ENASE*, pp. 344-354, 2022.

- [19] M.-C. Jakobs, "Automatic Test-Case Generation with CoVeriTest (Extended Abstract)," Cham, 2022, pp. 3-8.
- [20] L. Raamesh, S. Radhika, and S. Jothi, "Generating Optimal Test Case Generation Using Shuffled Shepherd Flamingo Search Model," *Neural Processing Letters*, vol. 54, pp. 5393-5413, 2022.
- [21] E. Jabbar, S. Zangeneh, H. Hemmati, and R. Feldt, "Test2Vec: An Execution Trace Embedding for Test Case Prioritization," *arXiv preprint arXiv:2206.15428*, 2022.
- [22] S. Anand, E. K. Burke, T. Y. Chen, J. Clark, M. B. Cohen, W. Grieskamp, *et al.*, "An orchestrated survey of methodologies for automated software test case generation," *Journal of Systems and Software*, vol. 86, pp. 1978-2001, 2013.
- [23] A. Issa, J. Sillito, and V. Garousi, "Visual testing of Graphical User Interfaces: An exploratory study towards systematic definitions and approaches," in *2012 14th IEEE International Symposium on Web Systems Evolution (WSE)*, 2012, pp. 11-15.
- [24] E. Alégroth, R. Feldt, and L. Ryrholm, "Visual GUI testing in practice: challenges, problems and limitations," *Empirical Software Engineering*, vol. 20, pp. 694-744, 2015.
- [25] E. Borjesson and R. Feldt, "Automated System Testing Using Visual GUI Testing Tools: A Comparative Study in Industry," in *2012 IEEE Fifth International Conference on Software Testing, Verification and Validation*, 2012, pp. 350-359.
- [26] V. Garousi, W. Afzal, A. Çağlar, İ. B. Işık, B. Baydan, S. Çaylak, *et al.*, "Comparing automated visual GUI testing tools: an industrial case study," presented at the Proceedings of the 8th ACM SIGSOFT International Workshop on Automated Software Testing, Paderborn, Germany, 2017.
- [27] B. Zitová and J. Flusser, "Image registration methods: a survey," *Image and Vision Computing*, vol. 21, pp. 977-1000, 2003.
- [28] X. Cao, J. Fan, P. Dong, S. Ahmad, P.-T. Yap, and D. Shen, "Chapter 14 - Image registration using machine and deep learning," in *Handbook of Medical Image Computing and Computer Assisted Intervention*, S. K. Zhou, D. Rueckert, and G. Fichtinger, Eds., ed: Academic Press, 2020, pp. 319-342.
- [29] M. V. Wyawahare, P. M. Patil, and H. K. Abhyankar, "Image registration techniques: an overview," *International Journal of Signal Processing, Image Processing and Pattern Recognition*, vol. 2, pp. 11-28, 2009.
- [30] N. Andrade, F. A. Faria, and F. A. M. Cappabianco, "A Practical Review on Medical Image Registration: From Rigid to Deep Learning Based Approaches," in *2018 31st SIBGRAP Conference on Graphics, Patterns and Images (SIBGRAP)*, 2018, pp. 463-470.
- [31] G. Haskins, U. Kruger, and P. Yan, "Deep learning in medical image registration: a survey," *Machine Vision and Applications*, vol. 31, p. 8, 2020.
- [32] X. Chen, A. Diaz-Pinto, N. Ravikumar, and A. F. Frangi, "Deep learning in medical image registration," *Progress in Biomedical Engineering*, vol. 3, p. 012003, 2021.
- [33] H. Xiao, X. Teng, C. Liu, T. Li, G. Ren, R. Yang, *et al.*, "A review of deep learning-based three-dimensional medical image registration methods," *Quant Imaging Med Surg*, vol. 11, pp. 4895-4916, 2021.
- [34] S. Bharati, M. Mondal, P. Podder, and V. Prasath, "Deep learning for medical image registration: A comprehensive review," *arXiv preprint arXiv:2204.11341*, 2022.
- [35] A. Sotiras, C. Davatzikos, and N. Paragios, "Deformable Medical Image Registration: A Survey," *IEEE Transactions on Medical Imaging*, vol. 32, pp. 1153-1190, 2013.
- [36] D. Lu, G. Li, and E. Moran, "Current situation and needs of change detection techniques," *International Journal of Image and Data Fusion*, vol. 5, pp. 13-38, 2014.
- [37] M. Hussain, D. Chen, A. Cheng, H. Wei, and D. Stanley, "Change detection from remotely sensed images: From pixel-based to object-based approaches," *ISPRS Journal of Photogrammetry and Remote Sensing*, vol. 80, pp. 91-106, 2013.

- [38] A. Varghese, J. Gubbi, A. Ramaswamy, and P. Balamuralidhar, "ChangeNet: A deep learning architecture for visual change detection," in *Proceedings of the European conference on computer vision (ECCV) workshops*, 2018.
- [39] B. D. de Vos, F. F. Berendsen, M. A. Viergever, H. Sokooti, M. Staring, and I. Išgum, "A deep learning framework for unsupervised affine and deformable image registration," *Medical Image Analysis*, vol. 52, pp. 128-143, 2019.
- [40] S. Wang, D. Quan, X. Liang, M. Ning, Y. Guo, and L. Jiao, "A deep learning framework for remote sensing image registration," *ISPRS Journal of Photogrammetry and Remote Sensing*, vol. 145, pp. 148-164, 2018.
- [41] K. Kuppala, S. Banda, and T. R. Barige, "An overview of deep learning methods for image registration with focus on feature-based approaches," *International Journal of Image and Data Fusion*, vol. 11, pp. 113-135, 2020.
- [42] A. Dhillon and G. K. Verma, "Convolutional neural network: a review of models, methodologies and applications to object detection," *Progress in Artificial Intelligence*, vol. 9, pp. 85-112, 2020.
- [43] A. Sotiras, Y. Ou, N. Paragios, and C. Davatzikos, "Graph-based Deformable Image Registration," in *Handbook of Biomedical Imaging: Methodologies and Clinical Research*, N. Paragios, J. Duncan, and N. Ayache, Eds., ed Boston, MA: Springer US, 2015, pp. 331-359.
- [44] M. R. Sabuncu and P. Ramadge, "Using Spanning Graphs for Efficient Image Registration," *IEEE Transactions on Image Processing*, vol. 17, pp. 788-797, 2008.
- [45] K. Deng, J. Tian, J. Zheng, X. Zhang, X. Dai, and M. Xu, "Retinal fundus image registration via vascular structure graph matching," *Journal of Biomedical Imaging*, vol. 2010, p. Article 14, 2010.
- [46] H. Jia, G. Wu, Q. Wang, Y. Wang, M. Kim, and D. Shen, "Directed graph based image registration," *Computerized Medical Imaging and Graphics*, vol. 36, pp. 139-151, 2012.
- [47] M. Moradi, K. Yan, D. Colwell, M. Samwald, and R. Asgari, "Model-agnostic explainable artificial intelligence for object detection in image data," *arXiv preprint arXiv:2303.17249*, 2023.